(Received 28 June 2024, Accepted 29 August 2024, Scheduled 7 September 2024)

Artificial Magnetic Conductor Based Improved Radiation Properties of Fractal MIMO Antenna for UWB Applications

Deshpande Ramesh, Yalavarthi Usha Devi*, and Boddapati T. P. Madhav

Department of ECE, Koneru Lakshmaiah Education Foundation, Vaddeswaram, AP, India

ABSTRACT: A novel artificial magnetic conductor (AMC) structure as a reflector is presented to enhance the gain of a fractal ultra-wideband (UWB) multi-input multi-output (MIMO) antenna. Unit cell of proposed AMC structure is achieved through 4 iterations to obtain better characteristics as reflector. An in-phase reflection from 2–16 GHz is achieved by the unit cell. The proposed AMC structure 6×6 array and 6×12 array are examined with single element and 2 element fractal MIMO antennas, respectively. The fractal MIMO antenna backed with an AMC structure achieved an operating band from 2.2 to 15.8 GHz, and the isolation between the elements is greater than 23 dB. The proposed AMC structure is fabricated, and experimental results are analysed in comparison with simulation ones. An average gain improvement of 6.1 dB is observed by the proposed AMC structure in the operating band. Surface current distributions, EM fields, and radiation patterns are investigated at various frequencies. MIMO performance parameters such as diversity gain, total active reflection coefficient, envelope correlation coefficient, and channel capacity loss characteristics are analyzed in this paper. The fractal MIMO antenna backed with an AMC structure exhibits good diversity performance characteristics with improved radiation properties for UWB applications.

1. INTRODUCTION

AMC is explored in various fields such as radar systems, telecommunications, internet of things (IoT) devices, and satellite communications in enhancing the gain of fractal antennas. It also provides more reliable wireless communication systems thereby enabling advancements in autonomous vehicles, medical monitoring, and remote sensing. Inclusion of AMCs also reduces surface wave propagation and backward radiation. Therefore, radiation efficiency of fractal antennas can be enhanced for good signal reception and transmission, particularly in environments with high attenuation or interference. Many researchers have worked on the design of various AMC structures for different applications and enhanced various properties of microstrip patch antennas. This section presents a brief review [1–29] of works done by various researchers in developing AMC structures. Novel broadband hexagon-shaped AMC and miniatured AMC are proposed for gain enhancement in [1, 2]. Various AMC structure designs and their applications on antennas have been presented for gain enhancement like polarization-insensitive AMC structure, stub-loaded artificial magnetic conductor, curved coupled microstrip line resonators based wideband uniplanar AMCs, and varactor-loaded AMC ground in [3–14]. AMC reflector for radio frequency identification (RFID) readers, AMC surface for vehicular wireless communications, AMC reflection phase characteristics, ultra-thin AMC, optically invisible AMC subarrays, RCS based on polarization-dependent AMC metasurface, compact tetracyclic nested AMC, etc. are proposed and analyzed in [15–29] for the gain enhancement of various microstrip patch antennas. From the literature review, most of the AMCs are proposed for narrowband applications. More research is required to develop wide band AMCs which can improve the radiation properties of fractal MIMO antennas over a wide frequency range.

This paper proposes a novel miniatured AMC to enhance the gain of UWB antennas. The proposed AMC is placed with a UWB fractal antenna and MIMO fractal antenna [30] to examine the behaviour with AMC and radiation properties like gain enhancement and radiation patterns. Section 2 describes AMC unit cell design and analysis with reflection and transmission coefficient characteristics. Section 3 presents the gain enhancement of a UWB fractal antenna using proposed AMC. Results are discussed in Section 4. The analysis of MIMO fractal antenna backed with AMC structure and MIMO performance metrics are illustrated in Sections 5 and 6. Section 7 concludes the proposed work with major findings.

2. AMC UNIT CELL AND ANALYSIS

UWB AMC structure as a reflector is proposed for enhancing the gain characteristics of UWB fractal antenna. The design of proposed AMC unit cell is carried out in four iterations as presented in Figure 1. Iteration-1 consists of the design of an AMC unit cell with square loop on a thin grounded dielectric substrate of dimensions $10 \times 10 \times 0.8\,\text{mm}^3$. It is designed on an FR-4 substrate with dielectric constant 4.4 and loss tangent 0.02 using ANSYS HFSS simulation tool. A three-hexagon element with side s_1 is integrated within the square loop in iteration-2, and a circle with diameter d_1 is etched from the center of hexagonal element in iteration-3. Parametric analysis is per-

* Corresponding author: Yalavarthi Usha Devi (ushadevi.yalavarthi@kluniversity.in).

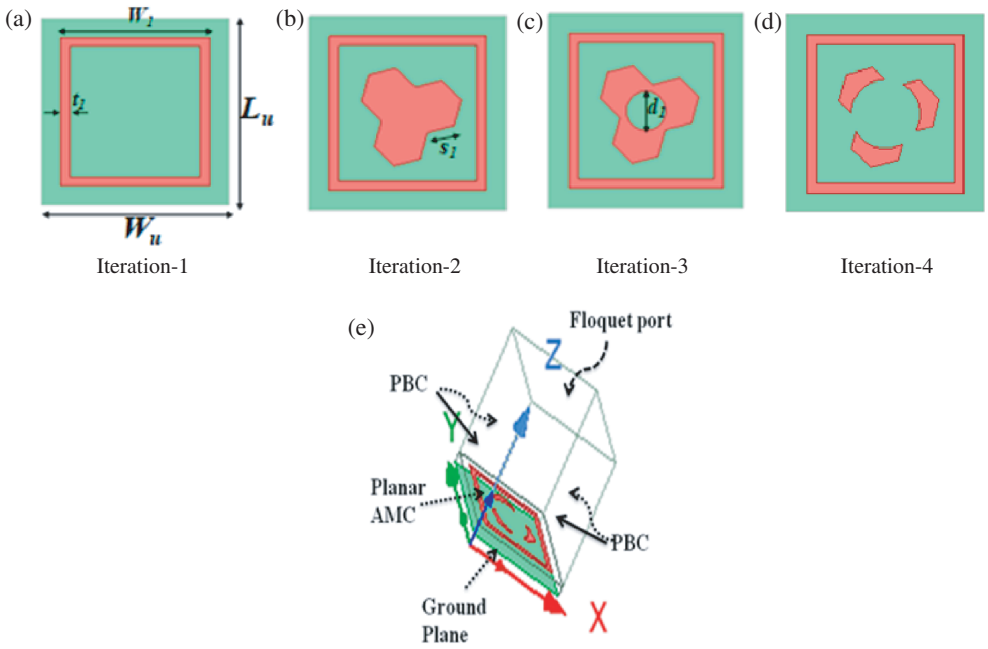

FIGURE 1. Iterations of AMC unit cell design.

formed on d_1 to further optimize the AMC unit cell design. For $d_1 = 4$ mm, AMC unit cell exhibits better S-parameter characteristics. Iteration-4 is the final proposed AMC unit cell with a UWB reflector. Geometrical specifications of the proposed AMC unit cell are tabulated in Table 1. Figure 1(e) illustrates the proposed AMC unit cell design and simulation model. Periodic boundary conditions (PBCs) are applied on the sides of unit cell to simulate an infinite array. Floquet port theory is used to analyze the unit cell reflection characteristics. In analyzing the AMC structure, the transmission coefficient (S_{21}) is omitted because the metallic ground plane inherent to the structure blocks any transmission. As depicted in Figure 1(e), adding a second Floquet port is impractical due to this ground plane. Consequently, only one Floquet port is used, positioned on the top surface of the AMC structure, to measure the reflection coefficient (S_{11}) and phase characteristics.

TABLE 1. Design parameters of proposed AMC unit cell.

Parameter	L_u	W_u	W_1	t_1	s_1	d_1
Dimensions in mm	10	10	8	0.5	1.41	2

The resonant frequency of the AMC is identified at 4.85 GHz. Reflection phase measurements were conducted at a distance of $\lambda/4 = 8.8$ mm (for center frequency 8.5 GHz) from the AMC surface using this single Floquet port configuration. The analysis presented in Section 2.1 centers on the reflection coefficient and phase characteristics, specifically for the TE mode.

2.1. Reflection and Transmission Coefficient Characteristics

S-parameter characteristics of the proposed AMC unit cell for iterations 1, 2, 3, and 4 are represented in Figure 2(a). From iteration-1 to iteration-4, reflection coefficient characteristics are improved to make the proposed AMC unit cell as a UWB reflector. Parametric analysis of iteration-3 with respect to the radius of etched circle 'r' ($d_1/2$) is depicted in Figure 2(b). 'r' is varied from 1 to 2.5 mm with a step size of 0.5 mm. For 'r' = 2 mm, the proposed AMC unit cell achieved better reflector characteristics in UWB frequency range. Figure 2(c) presents reflection phase characteristics of the proposed AMC unit cell. The reflection phase of the AMC structure was examined over a wide frequency range (2–16 GHz). The analysis revealed that the reflection phase transitions from -90 degrees to -180 degrees within 5 to 5.8 GHz band, signifying an out-of-phase reflection in this specific frequency range, and it achieved in-phase reflection band in the remaining frequency band that is most suitable to enhance radiation properties of UWB antennas.

3. ANTENNA GAIN ENHANCEMENT WITH PROPOSED AMC

To validate the performance of proposed AMC structure in gain enhancement, it is placed beneath a fractal UWB antenna [30], and the results obtained are analyzed. Figure 3 presents the placement of proposed AMC structure of 6×6 array simulation model and fabricated model. The simulation model top view of the fractal antenna placed over 6×6 array AMC is illustrated in Figure 3(a). The distance of separation between antenna and AMC is 'h' and can be observed in Figure 3(b). The proposed AMC is fabricated and examined experimentally as illustrated in Figure 3(c). Optimized separation between antenna and AMC is achieved through parametric analysis with respect to 'h'. Gain characteristics of the antenna with AMC for various values of 'h' = 12, 13, 14, and 15 mm are illustrated

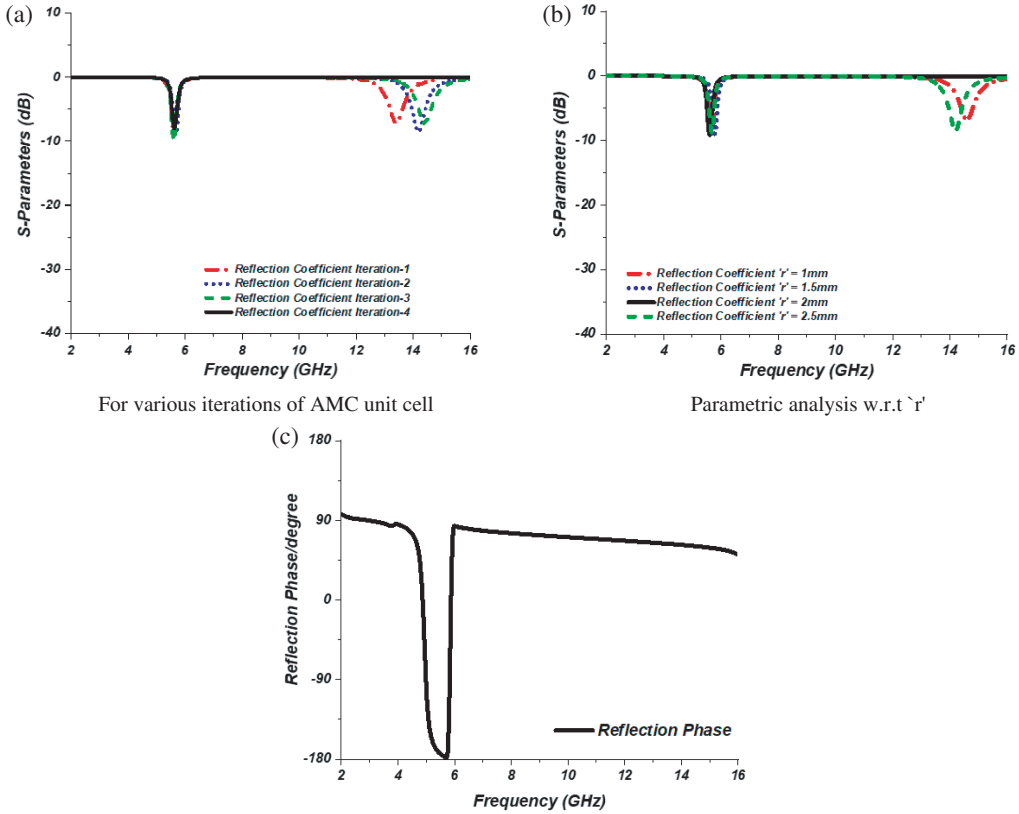

For various iterations of AMC unit cell

Parametric analysis w.r.t `r'

Reflection phase characteristics of iteration-4

FIGURE 2. S-parameter characteristics of proposed AMC unit cell.

in Figure 4. For $h = 14$ mm, it obtained better gain characteristics with a peak gain of 8.9 dB at 9.5 GHz. Gain values for various 'h' values at different resonant frequencies are presented in Table 2.

TABLE 2. Peak gain (dB) values at different frequencies for various 'h' values.

Frequency (GHz)	h = 12 mm	h = 13 mm	h = 14 mm	h = 15 mm
2.7	3.99	4.45	5.75	4.94
4.2	6.30	6.75	8.05	7.25
5.4	5.16	5.62	6.92	6.12
5.9	5.22	5.67	6.97	6.17
7.3	5.15	5.60	6.90	6.10
8.6	6.39	6.84	8.14	7.34
10.5	6.34	6.79	8.11	7.29
12.6	4.46	4.91	6.22	5.41

4. RESULTS AND DISCUSSION

4.1. S_{11} Characteristics

Figure 5 depicts measured and simulated S_{11} characteristics of the antenna backed with and without AMC. It operates for UWB from 2.25 GHz to 15.46 GHz with an impedance bandwidth ($S_{11} <= -10$ dB) of 13.21 GHz. Measured values using VNA slightly deviate from simulated values by maintaining UWB. S_{11} values at different frequencies are tabulated in Table 3.

TABLE 3. S_{11} values at different frequencies.

Frequency (GHz)	Simulated without AMC	Simulated with AMC	Measured with AMC
4.2	−14.51	−11.21	−12.78
5.9	−14.38	−21.01	−20.03
7.3	−10.69	−10.34	−13.74
8.6	−52.59	−26.92	−20.01
10.5	−24.11	−22.31	−18.52
12.6	−19.00	−33.30	−24.93

4.2. Surface Current Distribution

Surface current distribution and EM fields of the proposed AMC placed with a fractal antenna are represented in Figure 6 at two key frequencies 5.9 GHz, 7.3 GHz. It is observed that AMC acts as a good reflector as no radiation is being transmitted through AMC. However, at 5.9 GHz minor radiation is coupled to AMC which can be observed in S-parameter characteristics of the proposed AMC unit cell in Figure 2(a).

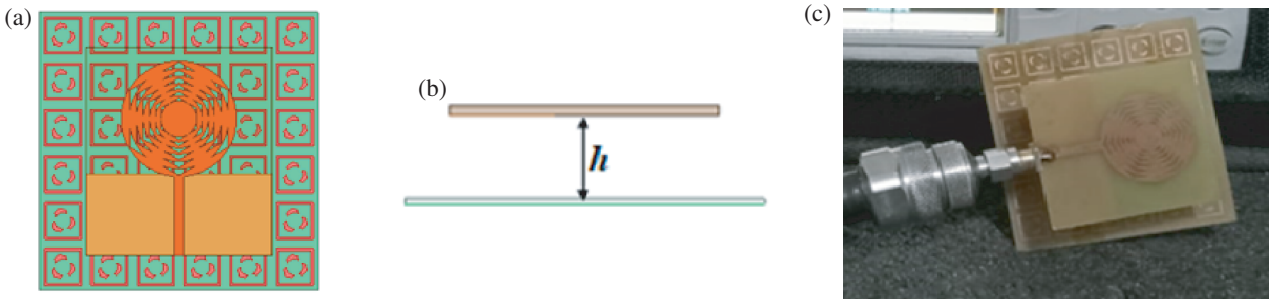

Top view of antenna placed over AMC | Side view of antenna and AMC | Fabricated antenna and AMC for testing

FIGURE 3. Placement of antenna on proposed AMC for gain enhancement.

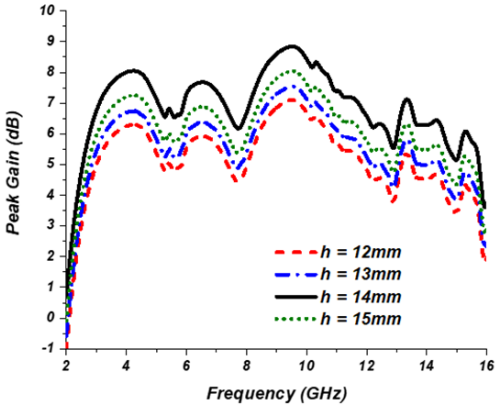

FIGURE 4. Gain characteristics for variations in 'h'.

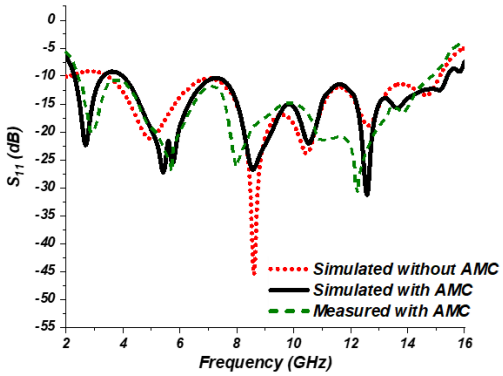

FIGURE 5. S_{11} characteristics.

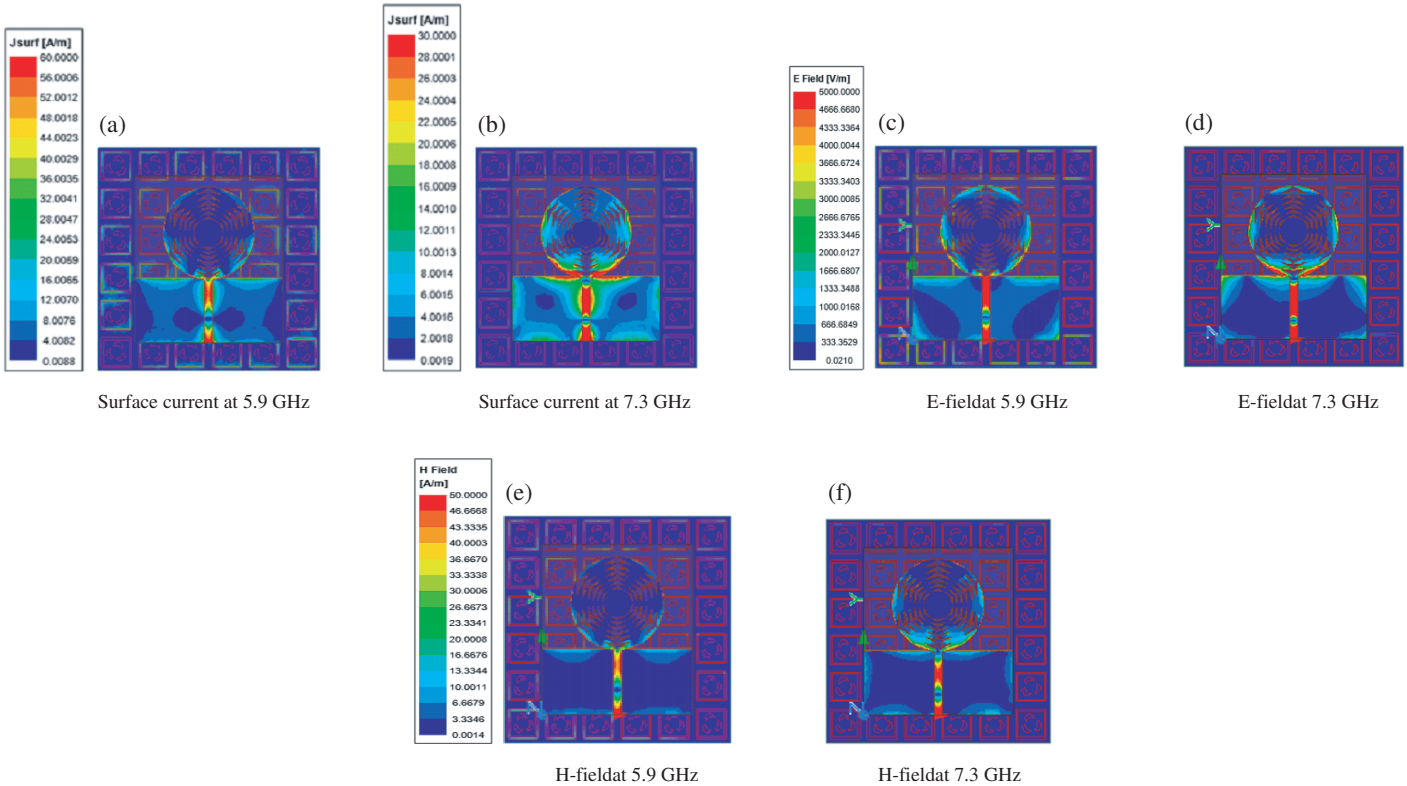

Surface current at 5.9 GHz | Surface current at 7.3 GHz | E-fieldat 5.9 GHz | E-fieldat 7.3 GHz

H-fieldat 5.9 GHz | H-fieldat 7.3 GHz

FIGURE 6. Surface current distribution and EM fields of antenna with AMC.

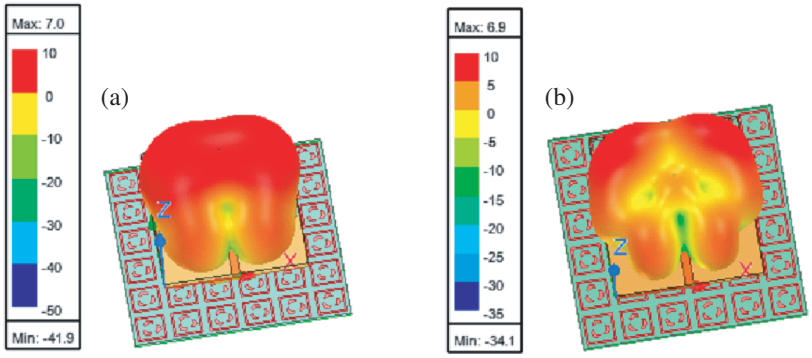

5.9 GHz 7.3 GHz

FIGURE 7. 3D gain plots of antenna with AMC.

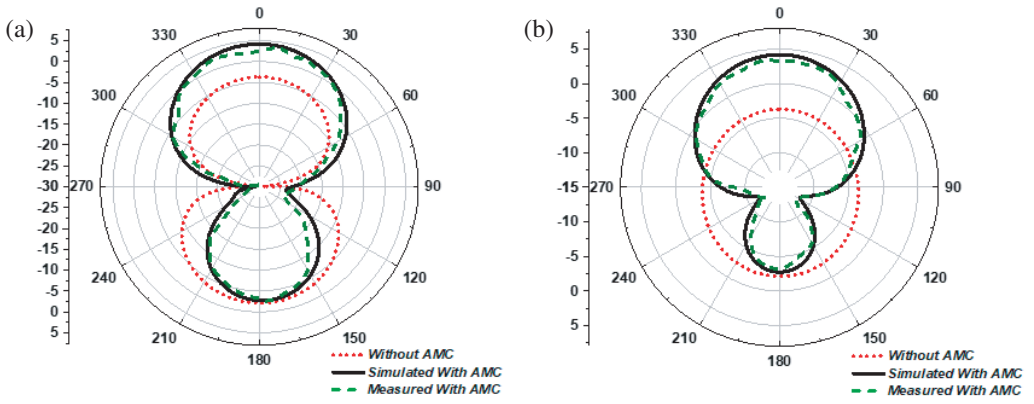

Phi 90 ^{o} at 2.4 GHz Phi 0 ^{o} at 2.4 GHz

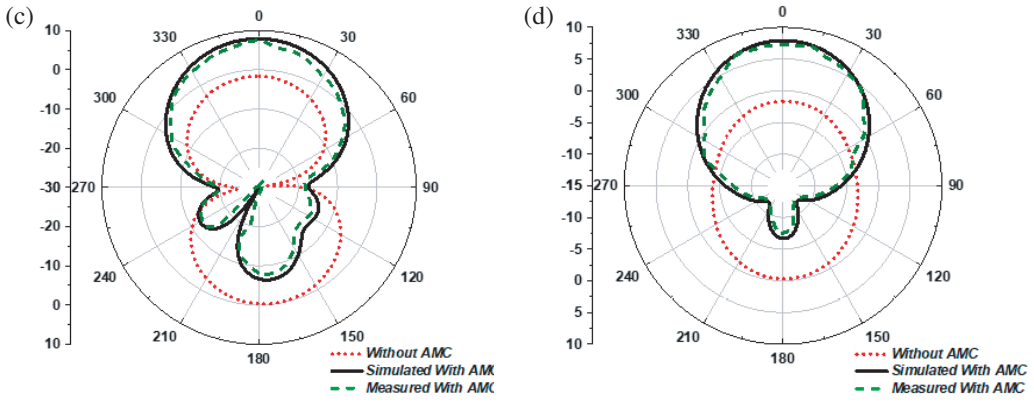

Phi 90 ^{o} at 3.8 GHz Phi 0 ^{o} at 3.8 GHz

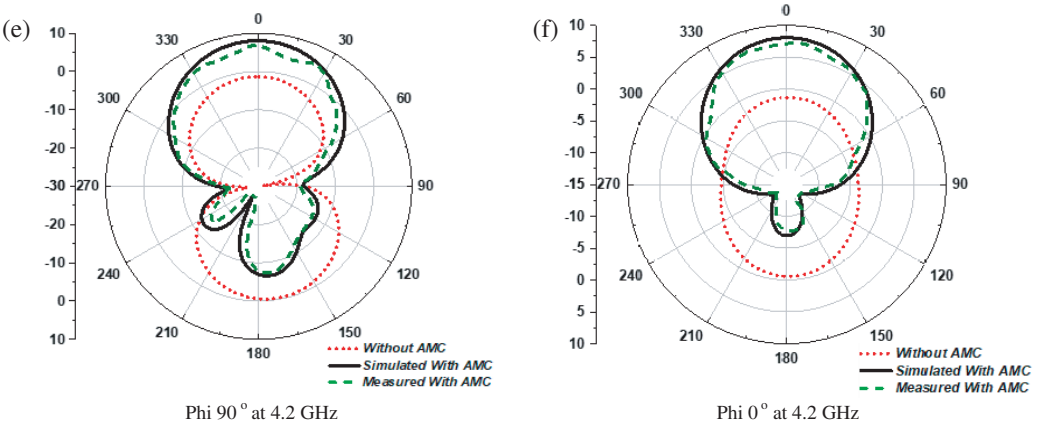

Phi 90 ^{o} at 4.2 GHz Phi 0 ^{o} at 4.2 GHz

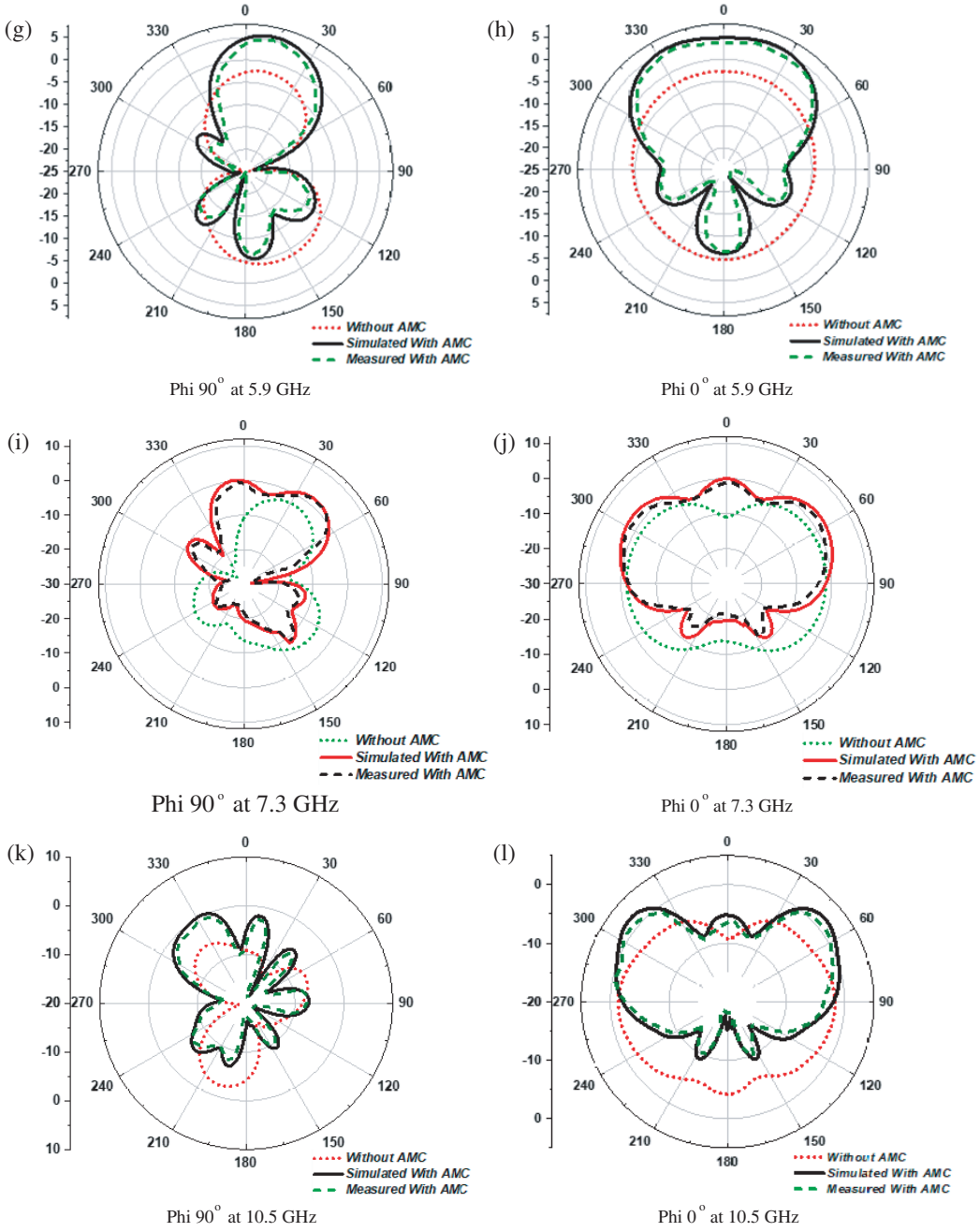

FIGURE 8. Radiation patterns at different frequencies with and without AMC.

4.3. Far-Field Radiation Characteristics

Figure 7 illustrates polar gain plots of the fractal antenna with AMC at 5.9 and 7.3 GHz. As AMC acts as a reflector, most of the back radiation is reflected towards forward direction, and therefore, gain of the fractal antenna is enhanced. AMCs exhibit a high surface impedance around their resonant frequency and result in constructive interference of the reflected waves. Therefore, the gain of antenna increases due to enhanced radiation in the desired direction. AMCs improve the gain of antenna by their unique properties like high surface impedance, surface wave suppression, and reduced back radiation.

Radiation patterns of the fractal antenna with and without AMC at various frequencies 2.4, 3.8, 4.2, 5.9, 7.3, and 10.5 GHz for Phi = 90° and Phi = 0° planes are plotted in Figures 8(a), (b), (c), (d), (e), (f), (g), (h), (i), (j), (k), and (l), respectively. From these patterns it can be observed how back radiation is reduced, and gain is enhanced in forward direction adding to major lobe with AMC. Figure 9 illustrates peak gain characteristics of the fractal antenna with and without AMC. At 5.9 GHz, the gain of fractal antenna without AMC is 0.2 dB, and with AMC the gain has improved to 6.3 dB. The reflection phase of the AMC structure indicates an out-of-phase reflection in 5–5.8 GHz frequency range. Despite this, gain enhance-

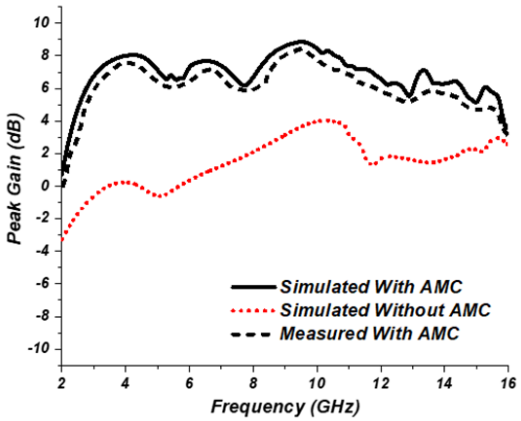

FIGURE 9. Simulated and measured gain characteristics with and without AMC.

ment is continuously observed from 2 to 16 GHz. Peak gain values of the fractal antenna with and without proposed AMC and improvement in gain are tabulated in Table 4 for some key frequencies.

TABLE 4. Peak gain values of fractal antenna.

Frequency (GHz)	Peak Gain (dB) without AMC	Peak Gain (dB) with AMC	Improvement in Gain (dB)
4.2	0.18	8.07	7.89
5.9	0.25	6.98	6.73
7.3	1.45	6.94	5.49
10	3.92	8.53	4.61
12	1.68	6.62	4.94

5. MIMO ANTENNA WITH AMC

Further, fractal MIMO antenna [30] is investigated for gain enhancement through the proposed AMC structure. Simulated model and fabricated prototype are presented in Figures 10(a) and (b). For fractal MIMO antenna, a 6×12 array AMC is implemented.

S-parameter characteristics of the MIMO antenna with and without AMC are presented in Figures 11(a) and (b). From reflection coefficient characteristics, it achieved an operating band from 2.2 GHz to 15.8 GHz with an impedance bandwidth of 13.6 GHz. The isolation between MIMO elements is greater than 23 dB with AMC as represented in transmission coefficient characteristics. Table 5 depicts the isolation between MIMO elements with AMC for different frequencies.

TABLE 5. Isolation between MIMO elements.

Frequency (GHz)	4.2	5.9	7.3	10	12
Isolation (dB)	27.5	25.4	30.7	42.2	32.1

Peak gain characteristics of fractal MIMO antenna with and without proposed AMC are presented in Figure 12(a). At 10 GHz frequency, gain is improved from 2.62 dB to 9.24 dB due to AMC. Peak gain values at various frequencies are tabulated in Table 6 with respective improvements in gain. Figure 12(b) illustrates the radiation efficiency characteristics of MIMO antenna across a frequency range of 2–16 GHz. The graph compares the simulated and measured radiation efficiencies for the antenna with and without AMC. Noticeable dip can be observed in out-of phase band due to the resonant effects of AMC. Radiation efficiency decreases at higher frequencies due to increased losses.

TABLE 6. Peak gain values of fractal MIMO antenna.

Frequency (GHz)	Peak Gain (dB) without AMC	Peak Gain (dB) with AMC	Improvement in Gain (dB)
4.2	1.06	7.27	6.21
5.9	1.40	6.48	5.08
7.3	1.72	8.20	6.48
10	2.62	9.24	6.62
12	2.73	7.52	4.79

6. MIMO PERFORMANCE METRICS

Major performance metrics of MIMO antenna are: total active reflection coefficient (TARC), envelope correlation coefficient (ECC), channel capacity loss (CCL), and diversity gain (DG). ECC can be obtained using Equation (1) [31], and ECC characteristics of MIMO antenna backed with AMC are illustrated in Figure 13. ECC values are less than 0.01 through operating band. Equation (2) [31] gives relation between DG and ECC values. From Figure 13, DG of MIMO antenna with AMC is very close to 10.

$$ECC = \frac{\left|\int_0^{2\pi}\int_0^{\pi}\left(XPRE_{\theta 1}E^*_{\theta 2}P_\theta + E_{\varphi 1}E^*_{\varphi 2}P_\varphi\right)d\Omega\right|^2}{\int_0^{2\pi}\int_0^{\pi}\left(XPRE_{\theta 1}E^*_{\theta 1}P_\theta + E_{\varphi 1}E^*_{\varphi 1}P_\varphi\right)d\Omega \times \int_0^{2\pi}\int_0^{\pi}\left(XPRE_{\theta 2}E^*_{\theta 2}P_\theta + E_{\varphi 2}E^*_{\varphi 2}P_\varphi\right)d\Omega} \quad (1)$$

where XPR is cross-polar discrimination, defined as time-averaged vertical-to-horizontal power ratio. $E_{\theta 1}$, $E_{\theta 2}$ are θ (vertical) polarized complex radiation patterns of antenna-1 and antenna-2 of the system, and $E_{\varphi 1}$, $E_{\varphi 2}$ are φ (horizontal) polarized complex radiation patterns of antenna-1 and antenna-2 of the system.

$$DG = 10\sqrt{1-\rho^2} \quad (2)$$

where ρ is the complex cross correlation coefficient with $|\rho|^2 \approx ECC$.

TARC can be obtained from S-parameters using Equation (3) (for 2-port network), and it gives the effective operating band of MIMO antenna. TARC characteristics are illustrated in Figure 14.

$$\Gamma_a^t = \sqrt{\frac{\left(\left(|s_{11} + S_{12}e^{j\theta}|^2\right) + \left(|s_{21} + S_{22}e^{j\theta}|^2\right)\right)}{2}} \quad (3)$$

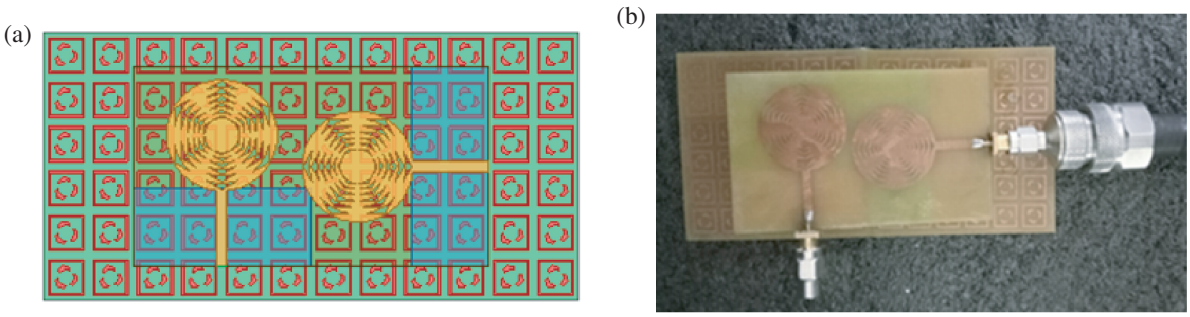

FIGURE 10. MIMO antenna over 6 × 12 array AMC.

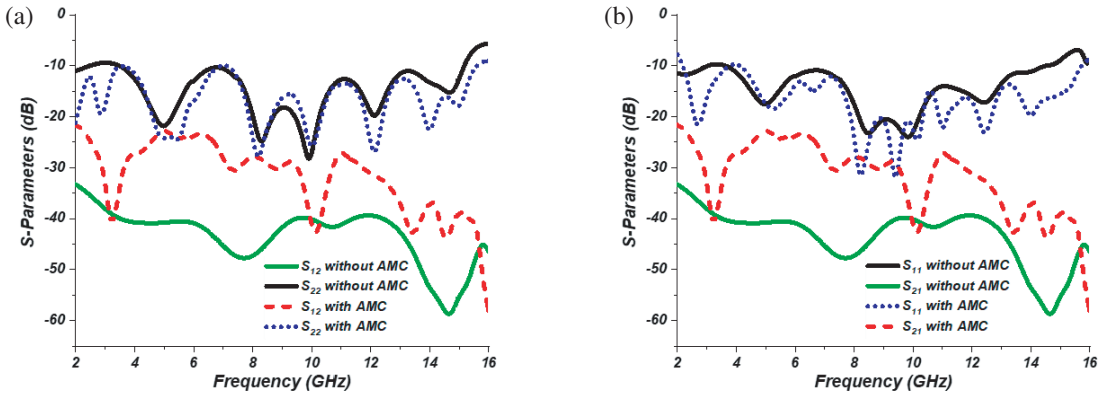

FIGURE 11. (a) S-parameter characteristics of MIMO antenna with and without AMC. (b) S-parameter characteristics of MIMO antenna with and without AMC.

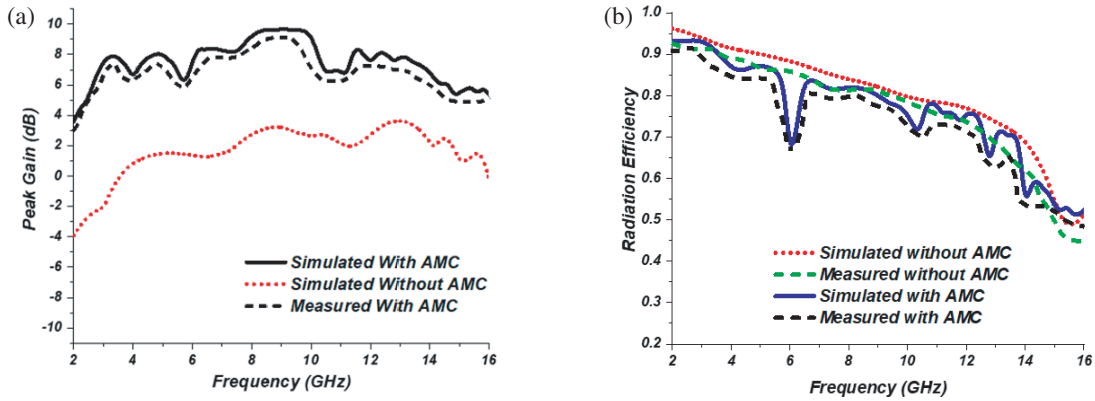

FIGURE 12. (a) Gain characteristics of MIMO antenna. (b) Radiation efficiency characteristics of MIMO antenna.

TABLE 7. Peak gain values of fractal antenna with and without AMC.

Frequency (GHz)	ECC	DG	CCL (bits/s/Hz)
4.2	0.0050	9.99987	0.37
5.9	0.0006	10	0.11
7.3	0.0005	10	0.31
10	0.0002	10	0.02
12	0.0007	10	0.06

where θ is the input feeding phase.

CCL defines the maximum limit for lossless transmission, and for CCL < 0.4 bits/s/Hz, lossless transmission is supported by MIMO antenna. CCL can be derived from S-parameters using Equations (4)–(9) for 2-port. Figure 14 illustrates that CCL values of the proposed fractal MIMO antenna backed with and CCL values are less than 0.4 bits/s/Hz in the operating band. ECC, DG, and CCL values for some key frequencies are tabulated in Table 7.

$$CCL = -\log_2(det(\psi^R)) \tag{4}$$

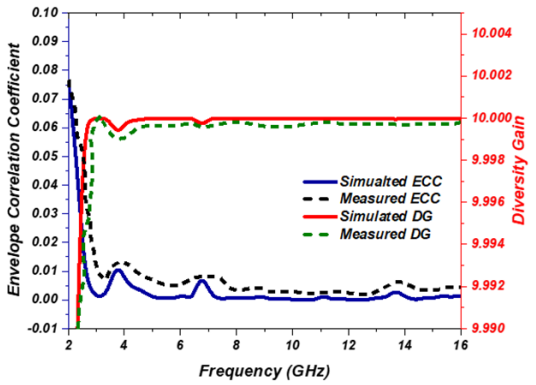

FIGURE 13. ECC and DG characteristics of MIMO antenna with AMC.

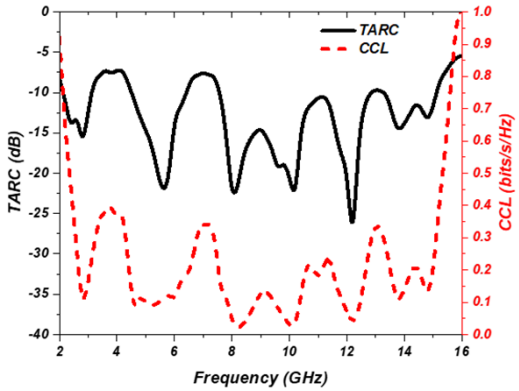

FIGURE 14. TARC and CCL characteristics of MIMO antenna with AMC.

TABLE 8. Comparison of proposed work with existing works.

Reference	MIMO elements	Operating Band (GHz)	Gain (dB)	Isolation (dB)	ECC	CCL (bits/sec/Hz)
[9]	2	3.0–4.1	7	> 25	< 0.01	-
[22]	-	4.77–7.12	9.9	-	-	-
[26]	-	3.2–11	7.2	-	-	-
[27]	4	3.3–6.02	8.4	> 30	-	-
Proposed work	2	2.2–15.8	8.5	> 23	< 0.01	< 0.4

where,

$$\psi^R = \begin{bmatrix} \rho_{11} & \rho_{12} \\ \rho_{21} & \rho_{22} \end{bmatrix} \quad (5)$$

$$\rho_{11} = 1 - \left(|S_{11}|^2 + |S_{12}|^2\right) \quad (6)$$

$$\rho_{22} = 1 - \left(|S_{22}|^2 + |S_{21}|^2\right) \quad (7)$$

$$\rho_{12} = -\left(S_{11}^* S_{12} + S_{21}^* S_{22}\right) \quad (8)$$

$$\rho_{21} = -\left(S_{22}^* S_{21} + S_{12}^* S_{11}\right) \quad (9)$$

The performance of the proposed AMC with fractal MIMO antenna is compared with existing literature review with respect to number of MIMO elements, operating band, gain, isolation, ECC, and CCL in Table 8.

7. CONCLUSION

A novel AMC structure is proposed to enhance the gain of fractal MIMO antenna for UWB applications. The proposed AMC structure is used as a reflector, and fractal single element antenna and MIMO antennas are examined for their performance. The fractal MIMO antenna bagged with AMC structure operates from 2.2 to 15.8 GHz, and gain has been improved to 8.5 dB. It also achieved good diversity performance. ECC is not greater than 0.01, and diversity gain is very close to 10. CCL is less than 0.4 bits/s/Hz, and the effective bandwidth obtained from total active reflection coefficient characteristics is also satisfactory for UWB applications. Therefore, the fractal MIMO antenna with proposed AMC structure exhibits enhanced radiation properties and good diversity performance suitable for UWB applications.

REFERENCES

[1] De Cos, M. E., Y. Alvarez, and F. Las-Heras, "Novel broadband artificial magnetic conductor with hexagonal unit cell," *IEEE Antennas and Wireless Propagation Letters*, Vol. 10, 615–618, 2011.

[2] Hadarig, R. C., M. E. D. Cos, and F. Las-Heras, "Novel miniaturized artificial magnetic conductor," *IEEE Antennas and Wireless Propagation Letters*, Vol. 12, 174–177, 2013.

[3] Prakash, P., M. P. Abegaonkar, A. Basu, and S. K. Koul, "Gain enhancement of a CPW-fed monopole antenna using polarization-insensitive AMC structure," *IEEE Antennas and Wireless Propagation Letters*, Vol. 12, 1315–1318, 2013.

[4] Yang, W., W. Che, and H. Wang, "High-gain design of a patch antenna using stub-loaded artificial magnetic conductor," *IEEE Antennas and Wireless Propagation Letters*, Vol. 12, 1172–1175, 2013.

[5] Yan, S., P. J. Soh, and G. A. E. Vandenbosch, "Low-profile dual-band textile antenna with artificial magnetic conductor plane," *IEEE Transactions on Antennas and Propagation*, Vol. 62, No. 12, 6487–6490, Dec. 2014.

[6] Saeed, S. M., C. A. Balanis, C. R. Birtcher, A. C. Durgun, and H. N. Shaman, "Wearable flexible reconfigurable antenna integrated with artificial magnetic conductor," *IEEE Antennas and Wireless Propagation Letters*, Vol. 16, 2396–2399, 2017.

[7] Rouzegar, S. M., A. Alighanbari, and O. M. Ramahi, "Wideband uniplanar artificial magnetic conductors based on curved coupled microstrip line resonators," *IEEE Microwave and Wireless*

Components Letters, Vol. 27, No. 4, 326–328, Apr. 2017.

[8] Yao, P., B. Zhang, and J. Duan, "A broadband artificial magnetic conductor reflecting screen and application in microstrip antenna for radar cross-section reduction," *IEEE Antennas and Wireless Propagation Letters*, Vol. 17, No. 3, 405–409, Mar. 2018.

[9] Zhu, J., S. Li, S. Liao, and Q. Xue, "Wideband low-profile highly isolated MIMO antenna with artificial magnetic conductor," *IEEE Antennas and Wireless Propagation Letters*, Vol. 17, No. 3, 458–462, Mar. 2018.

[10] Ghosh, A., V. Kumar, G. Sen, and S. Das, "Gain enhancement of triple-band patch antenna by using triple-band artificial magnetic conductor," *IET Microwaves, Antennas & Propagation*, Vol. 12, No. 8, 1400–1406, Mar. 2018.

[11] Bahari, N., M. F. Jamlos, and M. M. Isa, "Gain enhancement of microstrip patch antenna using artificial magnetic conductor," *Bulletin of Electrical Engineering and Informatics*, Vol. 8, No. 1, 166–171, 2019.

[12] Gong, Y., S. Yang, B. Li, Y. Chen, F. Tong, and C. Yu, "Multi-band and high gain antenna using AMC ground characterized with four zero-phases of reflection coefficient," *IEEE Access*, Vol. 8, 171 457–171 468, 2020.

[13] Liu, Q., H. Liu, W. He, and S. He, "A low-profile dual-band dual-polarized antenna with an AMC reflector for 5G communications," *IEEE Access*, Vol. 8, 24 072–24 080, Jan. 2020.

[14] Yang, S., Y. Chen, C. Yu, Y. Gong, and F. Tong, "Design of a low-profile, frequency-reconfigurable, and high gain antenna using a varactor-loaded AMC ground," *IEEE Access*, Vol. 8, 158 635–158 646, 2020.

[15] Sarkar, S. and B. Gupta, "A dual-band circularly polarized antenna with a dual-band AMC reflector for RFID readers," *IEEE Antennas and Wireless Propagation Letters*, Vol. 19, No. 5, 796–800, May 2020.

[16] Shi, S., P. Yang, W. Feng, L. Zhou, Q. Lu, W. Chen, and W. Che, "Wideband planar phased array antenna based on artificial magnetic conductor surface," *IEEE Transactions on Circuits and Systems II: Express Briefs*, Vol. 67, No. 10, 1909–1913, Oct. 2020.

[17] Malekpoor, H. and M. Hamidkhani, "Performance enhancement of low-profile wideband multi-element MIMO arrays backed by AMC surface for vehicular wireless communications," *IEEE Access*, Vol. 9, 166 206–166 222, 2021.

[18] Belabbas, K., D. Khedrouche, and A. Hocini, "Artificial magnetic conductor-based millimeter wave microstrip patch antenna for gain enhancement," *Journal of Telecommunications and Information Technology*, No. 1, 56–63, 2021.

[19] Jamali Arand, A. and B. A. Arand, "Performance enhancement of microstrip antenna using artificial magnetic conductor reflection phase characteristics," *International Journal of RF and Microwave Computer-Aided Engineering*, Vol. 31, No. 8, e22705, May 2021.

[20] Qiu, L. and G. Xiao, "An artificial magnetic conductor-based wideband circularly polarized antenna with low-profile and enhanced gain," *Electronics*, Vol. 10, No. 17, 2121, Aug. 2021.

[21] Fattouche, A., L. Mouffok, S. Hebib, and A. Mansoul, "A triple band artificial magnetic conductor: Design & analytical model," *Progress In Electromagnetics Research Letters*, Vol. 104, 161–168, 2022.

[22] Jiang, Z., Z. Wang, L. Nie, X. Zhao, and S. Huang, "A low-profile ultrawideband slotted dipole antenna based on artificial magnetic conductor," *IEEE Antennas and Wireless Propagation Letters*, Vol. 21, No. 4, 671–675, Apr. 2022.

[23] Yu, Y., Z. Akhter, and A. Shamim, "Ultra-thin artificial magnetic conductor for gain enhancement of antenna-on-chip," *IEEE Transactions on Antennas and Propagation*, Vol. 70, No. 6, 4319–4330, Jun. 2022.

[24] Nguyen, T. D., K. Kim, S. R. Yoon, and G. Byun, "Optically invisible artificial magnetic conductor subarrays for triband display-integrated antennas," *IEEE Transactions on Microwave Theory and Techniques*, Vol. 70, No. 8, 3975–3986, Aug. 2022.

[25] Ali, U., A. Basir, M. Zada, S. Ullah, B. Kamal, and H. Yoo, "Performance improvement of a dual-band textile antenna for on-body through artificial magnetic conductor," *IEEE Access*, Vol. 11, 72 316–72 331, 2023.

[26] Ibrahim, K. M., E. M. Eldesouki, and A. Attiya, "Compact ultra-wideband antenna backed by an artificial magnetic conductor," *Progress In Electromagnetics Research C*, Vol. 133, 251–260, 2023.

[27] Malekpoor, H., "AMC-loaded low-profile broadband printed 2×2 array with gain and isolation enhancement using equivalent circuit model for wireless systems," *IEEE Access*, Vol. 11, 22 007–22 017, 2023.

[28] Soliman, S. A. M., E. M. El-Desouki, S. M. El-Nady, and A. S. A. El-Hameed, "Broadband low rcs based on polarization-dependent artificial magnetic conductor metasurface," *IEEE Access*, Vol. 11, 53 176–53 184, 2023.

[29] Yang, S., F. Tong, J. Chu, Y. Chen, Z. Zhao, Z. Fang, Y. Zheng, and W. Wang, "Compact tetracyclic nested AMC-backed multi-band antenna with high OoB rejection and enhanced gain radiation for IIoV-based sensing and communication," *IEEE Internet of Things Journal*, Vol. 11, No. 2, 2819–2829, Jan. 2024.

[30] Deshpande, R. and U. D. Yalavarthi, "Hexa-slot wheel shaped fractal orthogonal MIMO antenna with polarization diversity for UWB applications," *Progress In Electromagnetics Research Letters*, Vol. 116, 31–38, 2024.

[31] El Ouahabi, M., A. Zakriti, M. Essaaidi, A. Dkiouak, and H. Elftouh, "A miniaturized dual-band MIMO antenna with low mutual coupling for wireless applications," *Progress In Electromagnetics Research C*, Vol. 93, 93–101, 2019.